

A GEANT3 Simulation of Pierre Auger Surface Detector Response to Muons

W. E. Slater, A. Tripathi, K. Arisaka
University of California, Los Angeles

7 November 2002

Abstract

Results of a GEANT3 based simulation of the response of Auger surface detectors are presented. We show that the ratio between the "muon hump" and VEM positions is affected by the photo-statistics. In the limiting case of large photo-statistics, this ratio is equal to 1 if sum of the three PMT signals is used. However, for realistic photostatistics, this number is closer to ~ 1.1 . We also show the behavior of the VEM pulse decay constant as a function of Tyvek reflectivity and water absorption length.

Table of Contents

1. Introduction.....	3
2. The Simulation.....	4
3. The "Muon Hump"/VEM Ratio.....	10
4 Pulse Decay Constants for Different Tyvek Reflectivity and Water Attenuation Lengths.....	13
5 Summary And Conclusion.....	16
6 References.....	16

1.Introduction.

In order to convert the signals seen by Auger surface detectors to an absolute energy, the detectors must be calibrated using vertical through going muons (VEM). However, in real life, we can not measure this number directly, since the detectors don't have trigger paddles on the top and bottom. We can only measure the "muon hump" (Figure 1), resulting from the low-threshold coincidence of the three PMTs in a tank. We need to infer the position of VEM from this muon hump. Measurements done on some test tanks so far show [1, 2] that this ratio of the "muon hump" to VEM is 1.12-1.15, if the sum signals of all three PMTs are used. For individual PMT signals, this ratio is ~ 1 [1,2]. In the rest of this document, the scintillator paddle trigger that gives rise to VEM will also be referred to as the "external trigger", and the trigger with simple 3-fold coincidence of the three PMTs in a tank will be referred to as the "internal trigger".

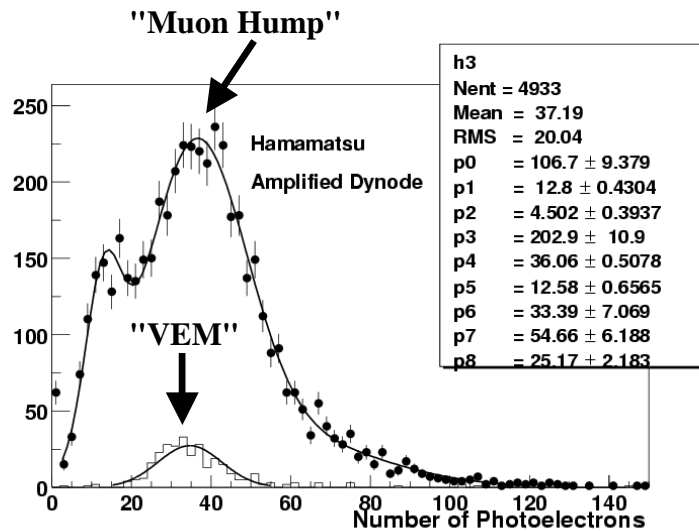


Figure 1: Typical PMT pulse area distributions showing both the VEM and the "muon hump" resulting from a simple coincidence of the three PMTs in a tank. These plots were made using data from the Fermilab tank.

Since any measurement errors in this ratio will directly translate into an error in the resulting shower energy by the same percentage amount, it is important to be able to simulate the detector response to both vertical and omni-directional muons in order to understand this ratio better.

This note shows close agreement of a GEANT3-based simulation of the Auger surface detector response with current experimental data from cosmic ray muons. GEANT3 is a time-tested package, and is much faster than its object oriented version, GEANT4.

In many of the distributions in this note, the abscissa is the simulated number of photoelectrons in an event. The gain of the phototube itself is not simulated, so the variable is strictly speaking not the FADC output. We will call this variable the photoelectron count (PEC for an acronym). Time distributions of these photoelectrons will be labeled TPE as they show the time of arrival at the pmt cathode of a cerenkov photon and may also be distorted by the propagation of electrons down the pmt dynode chain.

2. The Simulation

The simulation starts with muon generation according to $\cos^2(\text{zenith})$. Accordingly, $\cos^3(\text{zenith})$ is selected from uniform random numbers between 0 and 1. One cosine factor is due to the solid angle element and the other two to the desired \cos^2 distribution. The distribution is given in Figure 2. Azimuth is taken uniformly from 0 to 2π . The space distribution of tracks is taken as uniform on a horizontal plane coincident with the bottom of the tank. This plane extends to $\pm 5R$ in both x and y where $R=1.8$ meter is the tank radius. A scatterplot of these points is shown in Figure 3.

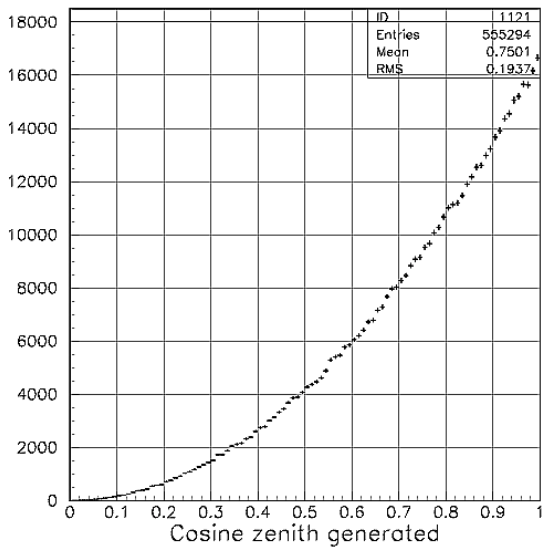


Figure 2: The distribution of the cosines of the zenith angles of the incident muons used in the simulation.

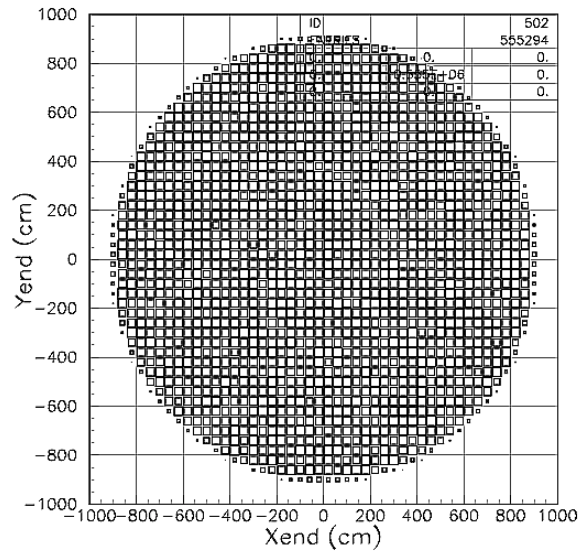


Figure 3: The distribution of the X and Y coordinates of all the tracks generated.

From that point, back along the direction already selected, a potential trajectory extends to a second plane at the tank top. This tentative muon path may or may not pass through the simulated tank. If not, the path is discarded. In case the path did pass through

the tank, a muon (both mu+ and mu- were run) was started at the intersection of the ray with the upper plane.

Most of the potential tracks are far from hitting the tank. A cut based on whether the starting point and ending point lie on the same side of the tank both in x and in y reduces the tracks to be followed by an order of magnitude. The candidates that pass this test are plotted in Figure 4. A few candidates appear out to the limits of the plot; these track vectors must have large horizontal components. One might expect a circular distribution of these points but Figure 4 is essentially square because the test is that a potential candidate track is declared followable based on its cartesian starting and ending coordinates; for both x and y, the starting and ending points must lie on opposite sides of the tank. Figure 5 shows the resulting exit points from the tank; most of them go out the bottom. The circular outline on the plot represents points exiting the cylinder sidewall.

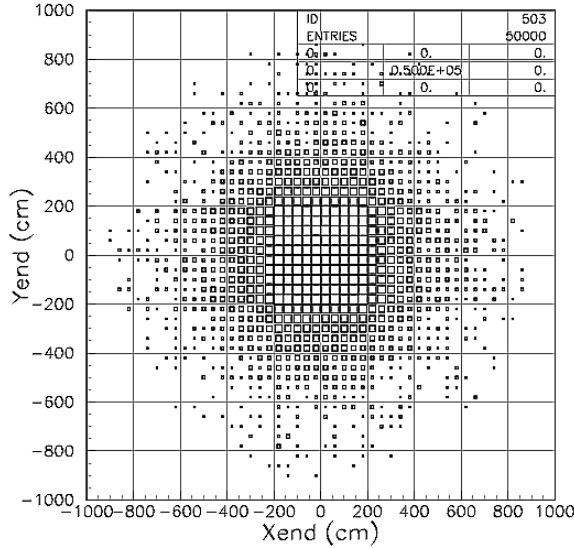


Figure 4: The distribution of the X and Y coordinates of the muons that were followed in the simulation.

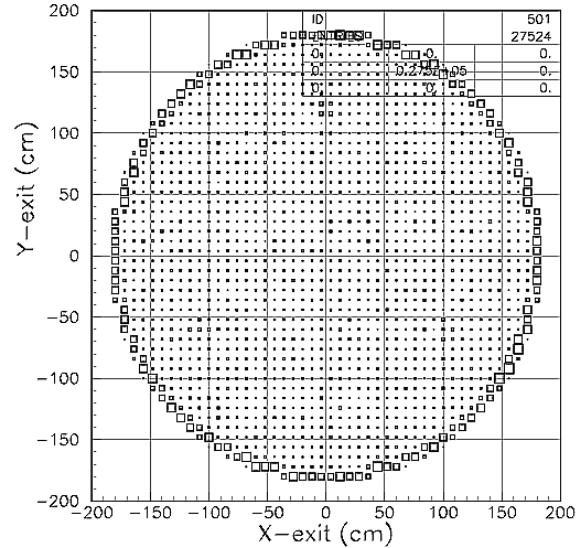


Figure 5: The distribution of the exit coordinates of the muons that were followed in the simulation.

Mu+ are characterized by their 2.2 microsecond meanlife; mu- were assigned an effective meanlife of 1.64 microsecond for water as measured by Sens. (Phys. Rev. 113, 679 [1959]) though the physics of the mu- capture process was not part of this simulation. Both charges were treated as if they would eventually decay so in particular the mu+ / mu- ratio was not studied. However, since there was no significant difference between mu+ and mu- events except for the time between muon and electron, nearly all of the runs were done with mu+. Water was designated as an optical medium for GEANT3 and Cerenkov photons between 1.9 ev and 5 ev (lambda between 250 and 670 nanometers) were generated for both the incoming muons and for decay electrons where relevant. The muon momentum spectrum is of great significance where decays are involved. We used

the distribution shown in Figure 6 having tabulated the numbers from experimental data first recorded in the 1950's (Manchester group, Handbuch der Physik). The built-in G3 photon tracing was very time consuming and was not used. Instead each photon inside the water was projected to the nearest Tyvek surface where a reflected photon of the same momentum was started. Photons could be dropped due to reflection inefficiency or to water absorption. A momentum-dependent PMT quantum efficiency loss was imposed. The QE characteristics for Photonis were measured as part of the UCLA PMT testing, and is used in these simulations.

The Photonis photocathode surfaces are nearly hemispherical with radius approximately 10 cm. In these simulations, the PMT was represented as a circle of radius 10-cm, which tends to underestimate photon acceptance and make this simulation somewhat pessimistic. The simulation did not include optical losses (reflection/refraction at the glass-water interface). These effects would reduce the acceptance so the simulation is optimistic in this regard. However, all these factors can be bundled together as the "effective QE", and we studied the detector response under various values of the effective QE.

The Cerenkov photon spectrum between the generated limits (1.9 to 4.5 ev already mentioned) is strongly modified by QE, attenuation, and reflectivity. The resulting spectrum is shown in Figure 7.

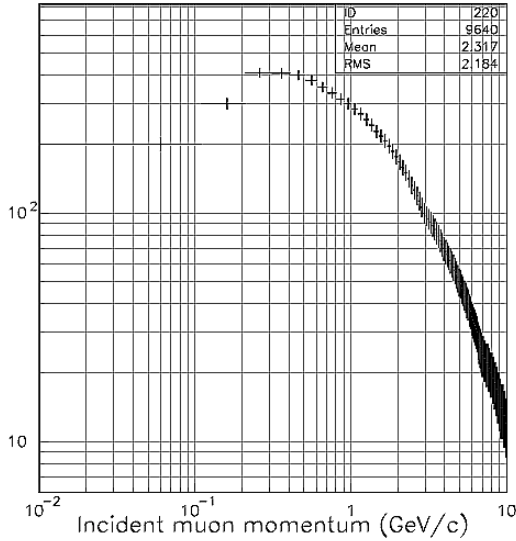


Figure 6: The momentum distribution used to generate the simulated muons

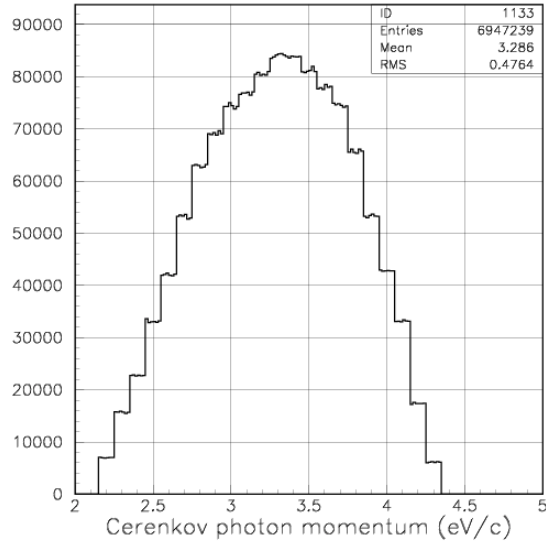


Figure 7: The momentum distribution of the Cerenkov photons, after QE, and attenuation in water.

The Tyvek reflectivity in air as well as in water has been studied experimentally [3, 4, 5, 6]. The effect on an incident photon is well described as the sum of two contributions:

- (1) Quasispecular. Photons are started with a gaussian spread (sigma about 18 degrees) around a specular reflected direction. Experimental fits found that the reflected “ray” is displaced by a very small amount (compared to 18 degrees) in average reflection angle. The measurement was done in the plane of incidence defined by normal to the Tyvek surface and the incident photon. This simulation generated a random azimuth around the specular ray.
- (2) Diffuse. Reflected photons were distributed as cosine theta, the angle with respect to the surface normal and with random azimuth around the surface normal. Again the reported measurement was done in the plane of incidence and reported a small deviation on average from the surface normal.

The relative contribution of the two terms was set to 1:1 for most of the simulation runs and no tuning was attempted in this simulation.

The experimental internal trigger for muon calibration is generated when all three PMTs see light at a level of 15% VEM. Accordingly, independent runs of the simulation found the average value of VEM for each single PMT and a threshold at 15% of this value was set. After that was programmed, any PMT was declared hit when the number of cerenkov photons to reach it in a 25 nanosecond interval crossed this threshold. To declare an event, all three PMTs had to be hit. The simulated PEC for each pmt was taken to be the sum of all cerenkov photons that reached it having passed losses to quantum efficiency, attenuation, and reflection.

The signal used for the trigger and PEC were strongly correlated as shown by Figure 8, a scatter-plot of these signals. The time distribution of the cerenkov photons is given in Figure 9. The early end has large fluctuation because there are events with less than 4 –5 bounces before a PMT is encountered. After the first few bins It is characterized by an exponential falloff with a slope of about 1/80 ns.

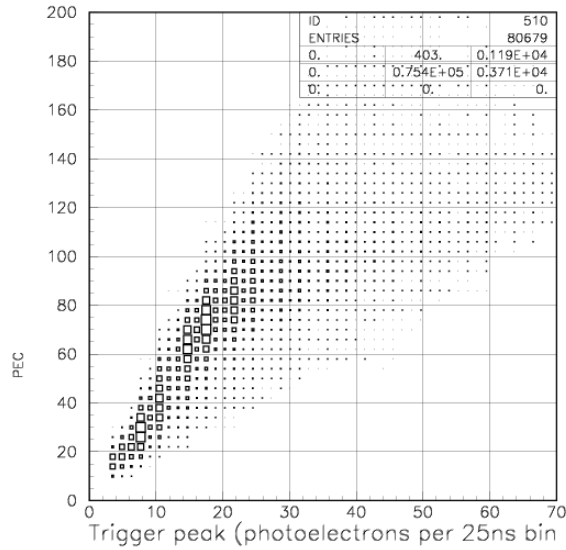


Figure 8: Correlation between the total number of photoelectrons seen by a PMT and the peak of the pulse caused by the muons.

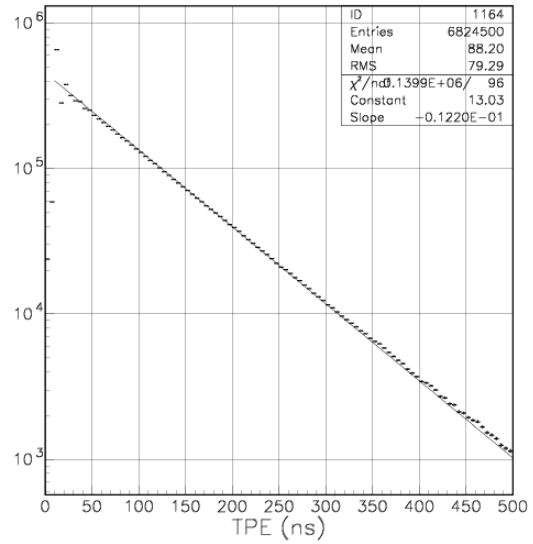


Figure 9: Distribution of the arrival times of the Cherenkov photons at the PMT.

A calibration in the field is expected to infer the signal for a vertical equivalent muon (VEM) from just the distribution of all muon signals. Much effort has been devoted to measuring these two FADC distributions in the laboratory. The G3 distribution of single PMT signals is given in Figure 10. Distribution from 100 MeV electrons is also superimposed (100 MeV is approximately the critical energy of the electrons in Air). Some of the muon decay events do not reveal separate positron and mu+ signals. These events add to the low end of this distribution. For Figure 10 the solid histogram came from a 100k event run on internal triggers. The points with error bars include a contribution from muon decays where a cerenk from a primary muon could add its signal to an internal trigger. The external trigger was based on placing 30-cm square apertures above and below the simulated tank.

Figure 10 already tells us that the "lower hump" seen in the data comes from the combination of the threshold effect on the omni-directional muons, decay electrons, and the soft EM component. It is NOT an artifact caused by any electronic noise or other extraneous factors. The muon flux at the lowest energies, which will also give rise to the decay electron, as well as the flux of the low energy EM component is not well known. As a result, the normalization at the lower end of the distributions shown in Figure 10 can be scaled up to obtain the distributions seen in real detector. Figure 11 shows the comparison of MC distribution obtained in this way with the data. The two distributions look quite similar, although the MC distribution is narrower. Clearly, by adjusting the amount of the low energy muon and EM component, as well as the photostatistics, the muon area distributions seen in real detectors can be easily reproduced.

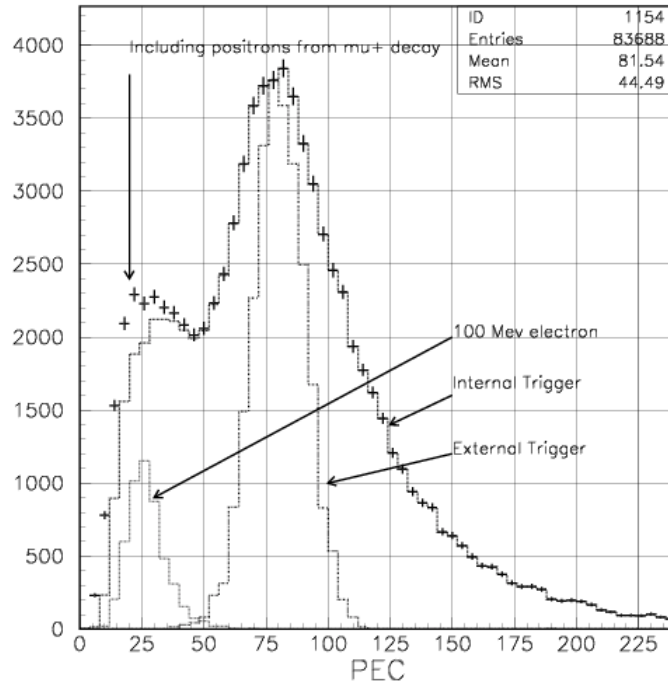


Figure 10: The photoelectron distributions obtained under various conditions. Clearly, the lower hump is a result of the soft EM component in the cosmic rays, as well as decay electrons. Only single PMT signals were used to make this plot.

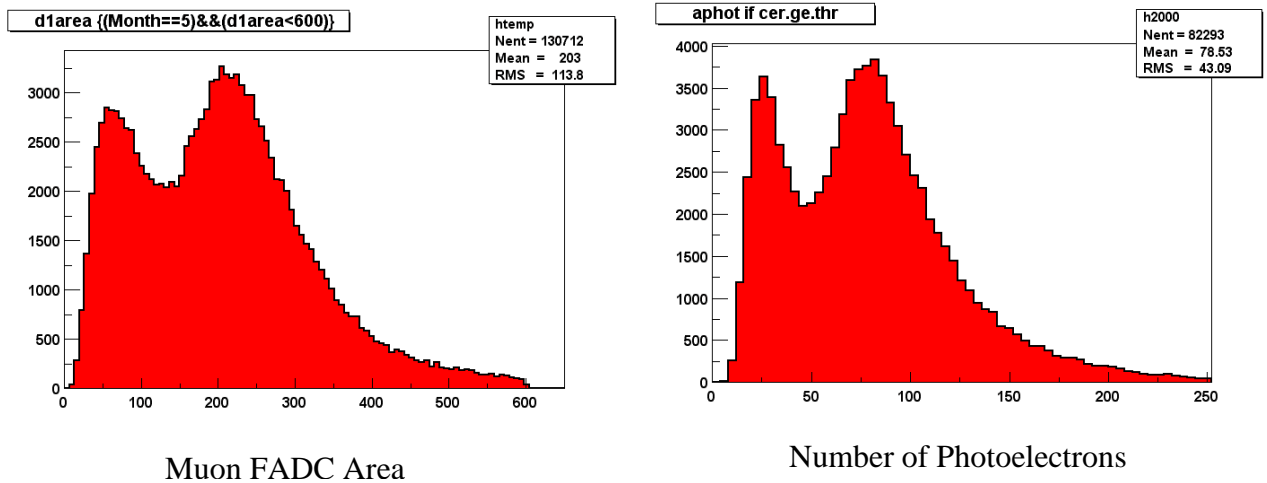


Figure 11 Comparison of single PMT muon area distributions obtained from real data (left panel, Tank46, PMT1, May 2002) and GEANT3 simulation (right panel). In the case of GEANT3 simulation, the amount of low-energy muon and soft EM component was adjusted by hand to obtain a distribution visually similar to the one obtained from real data.

3. The "Muon Hump"/VEM Ratio

In real Auger detectors, this ratio is found to be in the range of 1.12-1.15, if the sum signal from the three PMTs used. For individual PMTs, this ratio is nearly 1. In order to understand whether this number depends on the photo-statistics, both VEM and omni-directional muons were simulated for various effective quantum efficiencies. Figures 12 and 13 show the distributions obtained from VEM as well as omni-directional muons for different values of the effective QE. Single PMT signals (Figure 12) as well as the sum of the three PMT signals (Figure 13) is shown. Clearly, these ratios depend on the photostatistics.

Figure 14 shows the "Muon/Hump"/VEM ratio as a function of effective QE for both the single PMT signals as well as the three PMT sum signals. Clearly, this ratio depends on the photostatistics, and the effect is opposite for single PMT signals compared to the three PMT sum signals. For single PMT signal, this ratio is ~ 0.9 for high photostatistics, approaching 1 as the photostatistics becomes poorer. For the three PMT sum signals, however, this ratio is 1.0 for high photostatistics, and approaches 1.1 as the photostatistics becomes poorer. We can conclude from this that the measured "Hump/VEM" ratio of ~ 1.1 is a consequence of the smearing due to limited photostatistics. This is consistent with an independent analytical analysis [7].

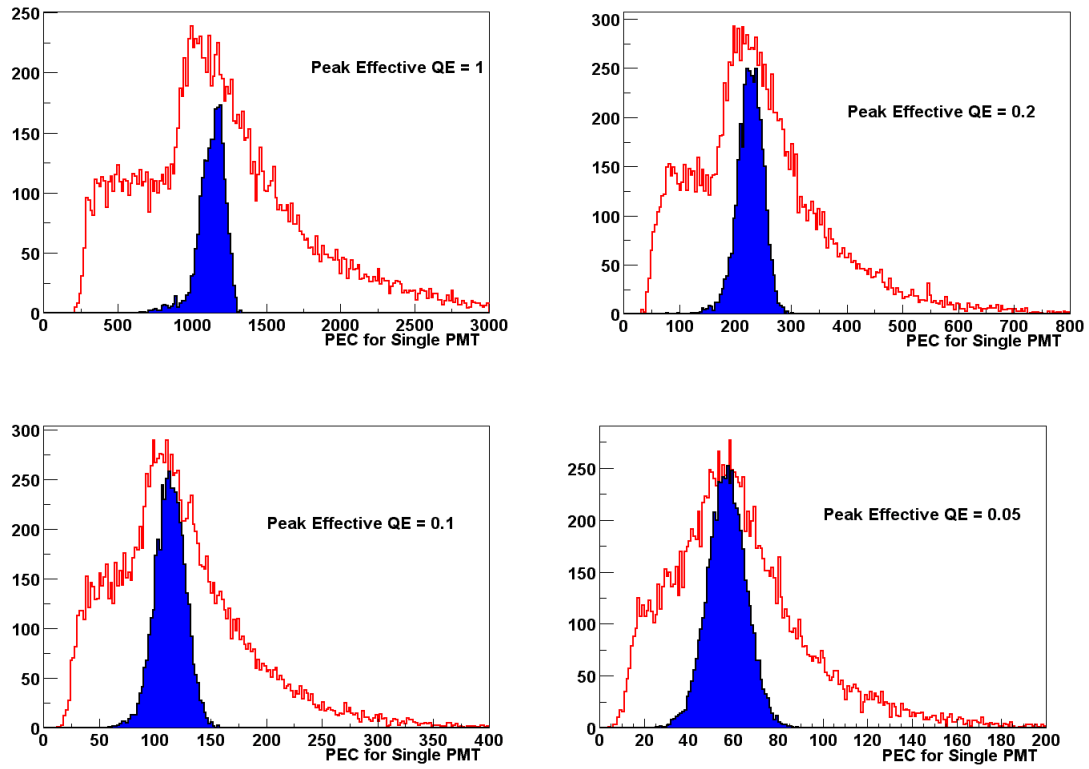


Figure 12: Single PMT signal distribution from VEM (filled, blue histograms) and omnidirectional (unfilled, red histograms) muons for various effective quantum efficiencies. Clearly, the ratio between muon hump and VEM depends on photostatistics.

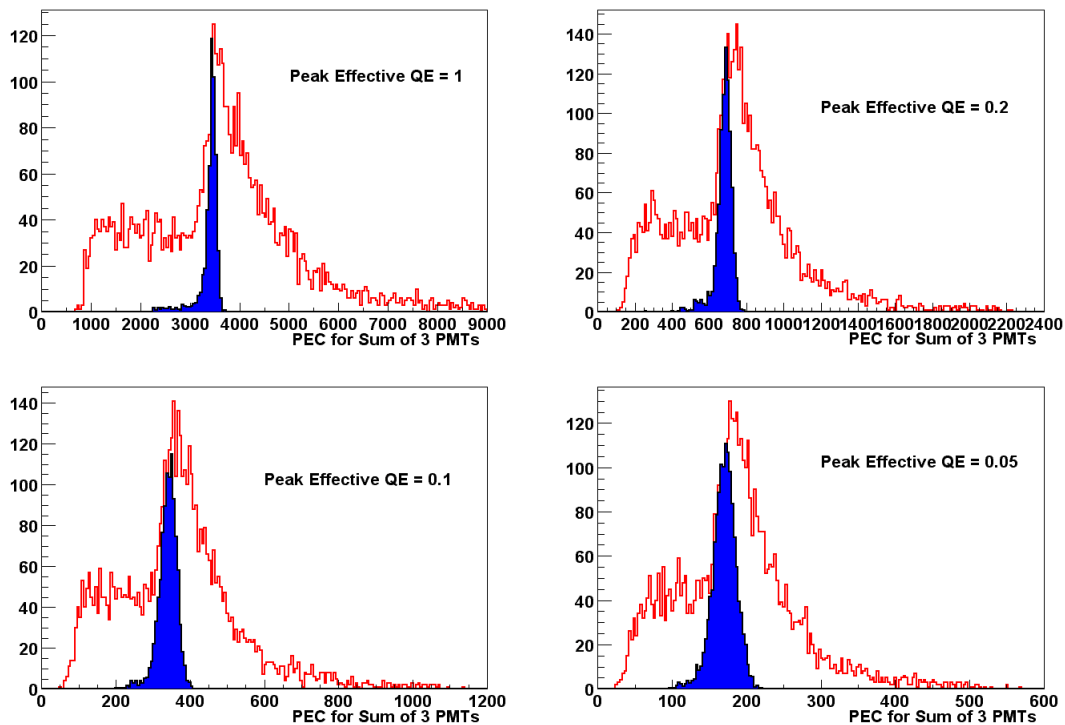


Figure 13: The three-PMT sum signal distribution from VEM (filled, blue histograms) and omni-directional (unfilled, red histograms) muons for various effective quantum efficiencies. Again, this ratio between muon hump and VEM depends on photostatistics.

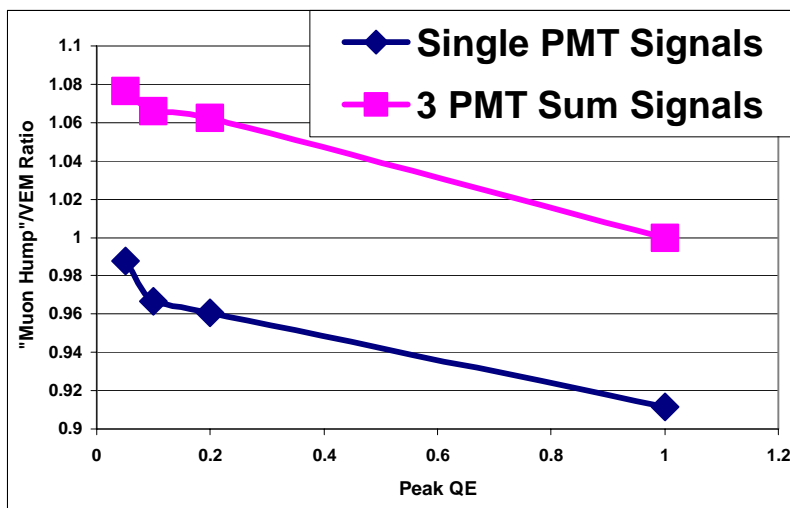


Figure 14: The "Muon Hump"/VEM ratio for various values of the effective QE; both for single PMT signals, as well as the 3 PMT sum signals.

4 Pulse Decay Constants for Different Tyvek Reflectivity and Water Attenuation Lengths

The pulse decay constant in Auger surface detectors can be and is used to monitor the tyvek reflectivity and water quality. In order to see how the pulse decay constant is affected by these changes, vertical muon simulations were carried out for various values of the Tyvek reflectivity and water attenuation lengths. The results are shown in Figures 15-18. One can see from these plots that Tyvek reflectivity affects the pulse height, area and decay constant much more than the water absorption length. For example, the Tyvek reflectivity dropping to 92% has the same effect as water absorption length dropping down to 10 m. This is an indication of the fact that the average path length between reflections is much smaller than typical water absorption lengths. Also, the pulse height is affected less than the pulse area, when either the Tyvek reflectivity or water absorption length changes. This is expected since the photons that make up the peak of the pulse arrive at the PMT after much fewer reflections than the photons in the rest of the pulse. And finally, the pulse decay constant is completely correlated with the "Area/Peak", as expected (Figure 19). So either quantity can be used to monitor the Tyvek reflectivity and water quality.

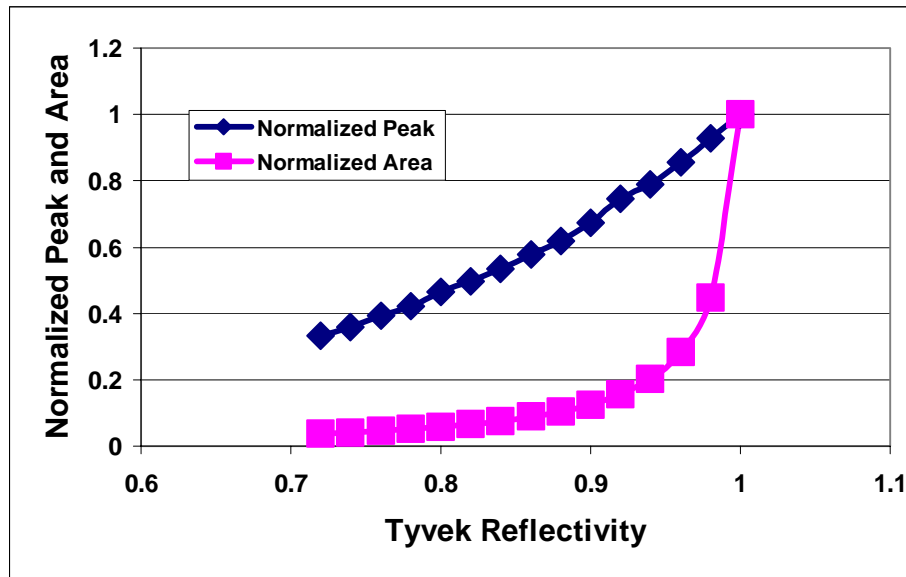


Figure 15: The VEM pulse height (peak) and pulse area as a function of Tyvek reflectivity. Both the peak and area have been normalized such that the maximum value is 1. The water attenuation length was fixed at 100 m for making this plot.

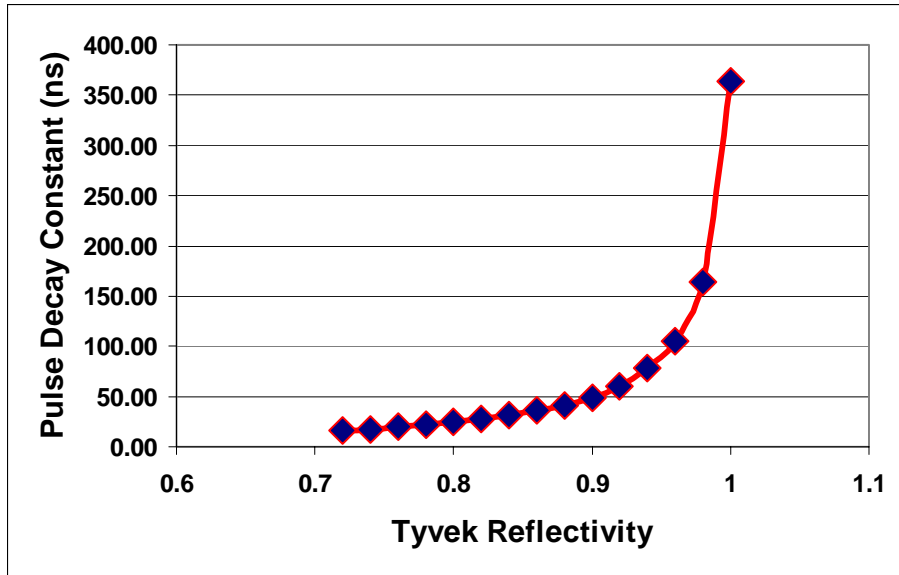


Figure 16: The VEM pulse decay constant as a function of Tyvek reflectivity. The water attenuation length was fixed at 100 m for making this plot.

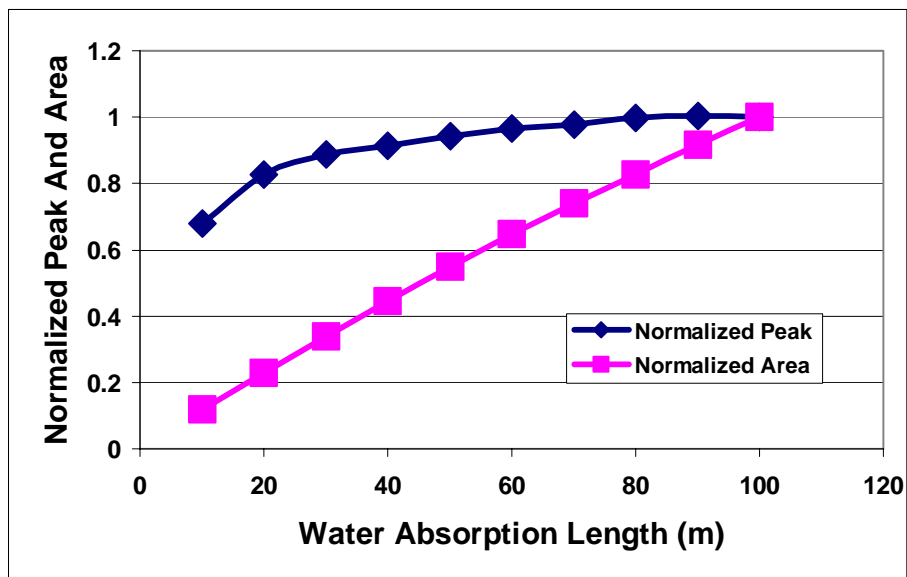


Figure 17: The VEM pulse height and pulse area as a function of water absorption length. The Tyvek reflectivity was fixed at 100% for making this plot.

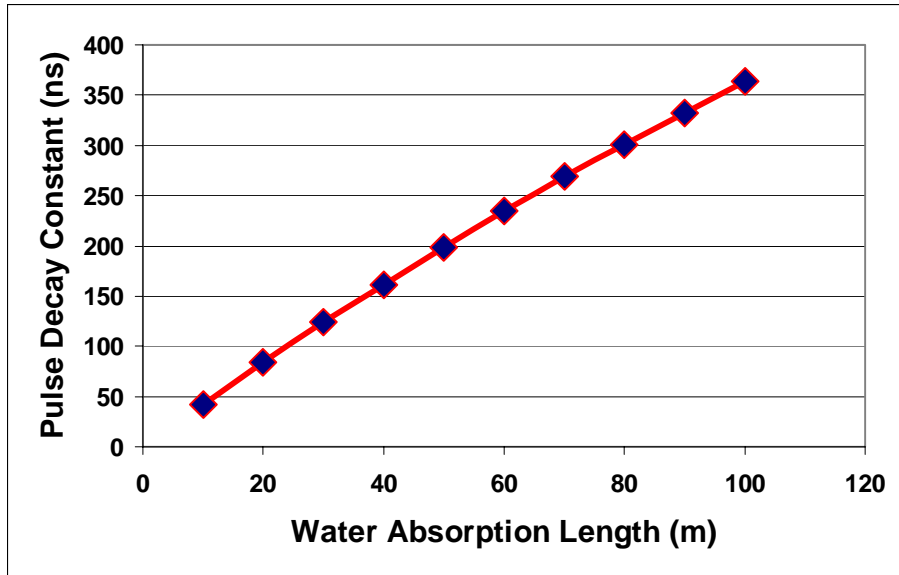


Figure 18: The VEM pulse decay constant as a function of water absorption length. The Tyvek reflectivity was fixed at 100% for making this plot.

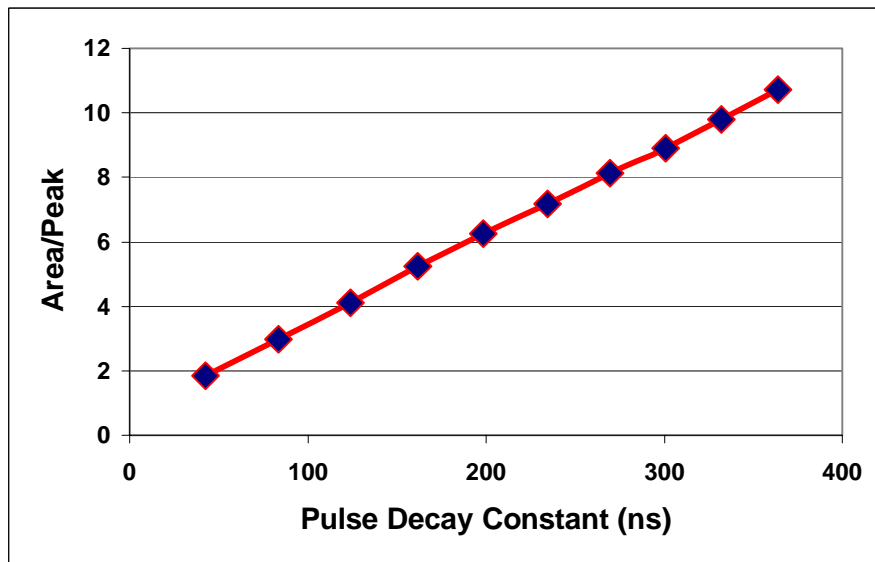


Figure 19: Correlation between (Area/Peak) and the pulse decay constant. As expected, the two are completely correlated.

5 Summary And Conclusion

We have performed a GEANT3 based simulation of the response of Auger surface detectors to muons and soft electromagnetic component under a variety of detector parameters, such as QE, tyvek reflectivity and water absorption length etc. We are able to reproduce the distributions observed in real detectors, both for vertical through going muons as well as omni-directional muons. We have shown that the "Muon Hump"/VEM ratio is affected by the photostatistics. This means that the measured ratio of 1.1-1.15 is a consequence of smearing due to limited photostatistics, and is not simply a property of the detector geometry.

6 References

1. P. S. Allison et al., "Surface Detector Calibration in the Engineering Array", Auger technical note **GAP-2002-028**.
2. A. S. Chou, "Vertical Equivalent Muon Study With the Fermilab Tank", Auger technical note **GAP-2002-045**.
3. C. Hojvat, "Comparison of the UV Reflectivity from Tyvek", Auger technical note **GAP-1996-007**.
4. F. Hasenbalg et al., "Tyvek Diffuse Reflectivity", Auger technical note **GAP-1997-035**.
5. A. Filevich et al., "Spectral-directional reflectivity of Tyvek immersed in water", Auger technical note **GAP-1997-065**.
6. J. C. Arteaga et al., "Diffuse Reflectivity of Tyvek in Air and Water, and Anisotropic Effects", Auger technical note **GAP-2000-035**.
7. A. Etchegoyen, "Track Geometry and Smearing of the Bump Calibration", soon to be submitted as a GAP note.